An Analytical Redundancy-Based Fault Detection and Isolation Algorithm for a Road-Wheel Control Subsystem in a Steer-By-Wire System

Sohel Anwar and Lei Chen

***Abstract*—This paper presents a novel observer-based analytical redundancy for a steer-by-wire (SBW) system. An analytical redundancy methodology was utilized to reduce the total number of redundant road-wheel angle (RWA) sensors in a triply redundant RWA-based SBW system while maintaining a high level of reliability. A full-state observer was designed using the combined model of the vehicle and SBW system to estimate the vehicle-body sideslip angle. The steering angle was then estimated from the observed and measured states of the vehicle (body sideslip angle and yaw rate) as well as the current input to the SBW electric motor(s). A fault detection and isolation (FDI) algorithm was developed using a majority voting scheme, which was then used to detect faulty sensor(s) to maintain safe drivability. The proposed analytical redundancy-based FDI algorithms and the linearized vehicle model were modeled in SIMULINK. Simulation results show that the proposed analytical redundancy-based FDI algorithm provides the same level of fault tolerance as in an SBW system with full hardware redundancy against single-point failures.**

***Index Terms*—Analytical redundancy, fault detection and isolation (FDI), road-wheel control system, steer-by-wire (SBW) system.**

I. Introduction

SAFETY, usability, and packaging benefits of drive-by-wire systems in an automobile have been well established over the last decade [1]. The challenge, however, remains in the reliability and fault tolerance of the by-wire systems [2]–[7]. Most fault-tolerant control systems require redundancy in the hardware components to make these systems more reliable. However, the additional components due to hardware redundancy make the cost of the overall drive-by-wire system excessively high. The concept of analytical redundancy has been investigated to replace some of the hardware redundancies, particularly in the context of aerospace applications, to reduce the overall cost and improve reliability [8]–[16]. However, most of these papers were aimed at isolated subsystems in an aircraft or a spacecraft. Fly-by-wire (FBW) systems are mostly based on full hardware redundancies. As a result, analytical redundancy methodologies have not been utilized to a great extent in FBW systems.

The theoretical foundation of analytical redundancy methodologies that have been researched in aerospace applications is believed to have a far-reaching impact on drive-by-wire systems. In this paper, we present the development of analytical redundancy methodologies for the fault tolerance of a steer-by-wire (SBW) system that is aimed at reducing the total number of redundant sensors without sacrificing the overall safety and performance of these systems. By reducing the total number of redundant components in an SBW system to a minimum set, the overall cost of such systems can be significantly reduced, making them production viable. The theoretical development in the analytical redundancy-based fault detection and isolation (FDI) methods for the SBW system can easily be carried over to the other by-wire systems for fault tolerance with a reduced number of hardware redundancies.

We first develop a steering system model to pave the way for developing analytical redundancy methodologies. Based on the steering system model, an observer is designed to estimate the road-wheel angle (RWA) based on the motor-current measurement. The observed value of the RWA is then used as the analytical sensor reading replacing one of the three redundant hardware sensors. Fault detection, isolation, and accommodation (FDIA) algorithms were also developed, based on the majority voting algorithm. The proposed analytical redundancy methodologies along with the FDIA algorithms were modeled in SIMULINK. A simplified vehicle model was also developed in SIMULINK to verify the proposed algorithms. A number of simulation runs were performed on the combined model for both transient and persistent sensor faults. Simulation results show that the analytical redundancy methods that are presented in this paper successfully detected both types of faults and provided the SBW controller with the correct value of the RWA value.

II. Steering System Model

Fig. 1 shows a configuration of an SBW system. The SBW system consists of a steering wheel (not mechanically

Manuscript received July 24, 2006; revised December 22, 2006 and December 25, 2006. This work was supported in part by an internal research grant from the Purdue School of Engineering and Technology, Indiana University-Purdue University Indianapolis, Indianapolis, IN. The review of this paper was coordinated by Dr. M. A. Masrur.

S. Anwar is with the Department of Mechanical Engineering, Purdue School of Engineering and Technology, Indiana University-Purdue University Indianapolis, Indianapolis, IN 46202 USA (e-mail: soanwar@iupui.edu).

L. Chen was with the Department of Electrical and Computer Engineering, Purdue School of Engineering and Technology, Indiana University-Purdue University Indianapolis, Indianapolis, IN 46202 USA (e-mail: leichen@iupui.edu.edu).

Color versions of one or more of the figures in this paper are available online at http://ieeexplore.ieee.org.

Digital Object Identifier 10.1109/TVT.2007.900515

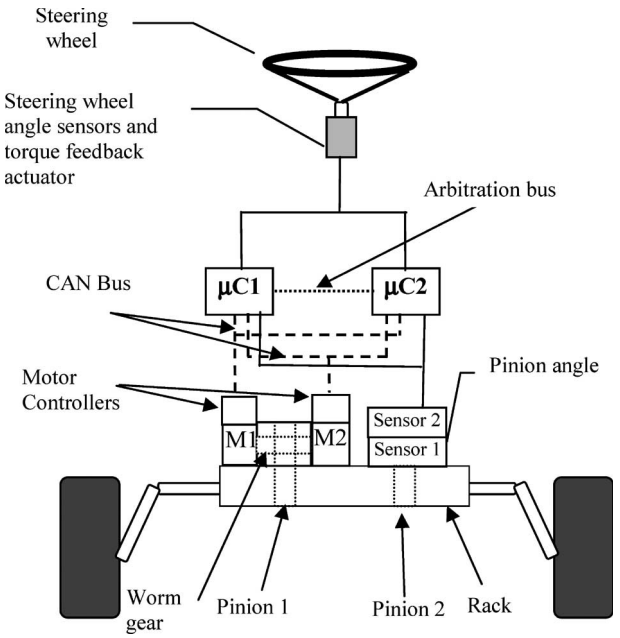

Fig. 1. SBW system.

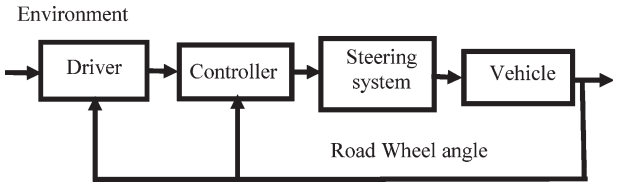

Fig. 2. SBW control system.

connected to the road wheels), a set of steering-wheel angle sensor attached to the steering wheel, a steering-wheel feedback actuator, electronic control units (ECUs), a set of road-wheel actuators (dc motors) connected to the rack-and-pinion assembly, and a set of RWA sensors. The SBW control system is illustrated in Fig. 2. The ECUs read the steering-wheel angle sensors and determine the road-wheel actuator and feedback actuator commands.

To develop the analytical redundancy, we first need to understand the steering dynamic. The steering system can be approximated by the following second-order equation [4]:

$$J_w\ddot{\theta} + b_w\dot{\theta} + F_c\text{sgn}(\dot{\theta}) + k_a\tau_a = n\tau_m \tag{1}$$

where

J_w moment of inertia of the road wheel;
b_w viscous damping coefficient;
F_c torque due to Coulomb friction force;
τ_a self-aligning torque;
k_a scaling factor;
τ_m total steering-motor torque;
θ RWA;
n number of road-wheel motors.

The self-aligning torque is due to the tire contact forces acting on the steering system to resist steering away from the straight-ahead position. The self-aligning moment can be calculated from

$$\tau_a = (t_p + t_m)F_{y,f}(\alpha_f) \tag{2}$$

where

t_p pneumatic trail;
t_m mechanical trail;
$F_{y,f}$ front-tire lateral force;
α_f front-tire sideslip angle.

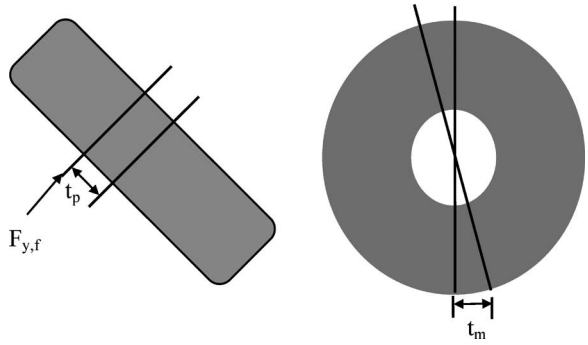

Fig. 3. (a) Pneumatic trail. (b) Mechanical trail.

The pneumatic trail is the distance between the tire center and the point where lateral force is applied, and the mechanical trail is the distance between the tire center and the point on the ground where the tire pivots as a result of caster angle (Fig. 3). Assuming a linear region of operation with front-tire sideslip angles less than 4°, the front-tire lateral force can be approximated as a function of the tire sideslip angle. The tire sideslip angle is the difference between the tire's longitudinal axis and the tire's direction of motion. It is very important because it gives the driver a sense of when the vehicle is reaching its handling limit. If the driver were to make a sharp turn at high speed, the driver would feel the vehicle losing lateral traction of the road, resulting in large sideslip angle. Therefore, it is desirable to keep the sideslip angle as small as possible.

Assuming a single SBW motor for simplicity $(n = 1)$, the SBW motor torque can be approximated as a function of the current i_m, where k_m is the motor constant. Thus

$$\tau_m = k_m i_m. \tag{3}$$

Rewriting (1) in a state-space form, we get the following equations:

$$\dot{x} = Ax + Bi_m + E\tau_a + F\tau_f$$

$$x = [\theta \quad \dot{\theta}]^T$$

$$A = \begin{bmatrix} 0 & 1 \\ 0 & -\frac{b_w}{J_w} \end{bmatrix} \quad B = \begin{bmatrix} 0 \\ \frac{k_m}{J_w} \end{bmatrix}$$

$$E = \begin{bmatrix} 0 \\ -\frac{1}{J_w} \end{bmatrix} \quad F = \begin{bmatrix} 0 \\ \frac{-1}{J_w} \end{bmatrix}. \tag{4}$$

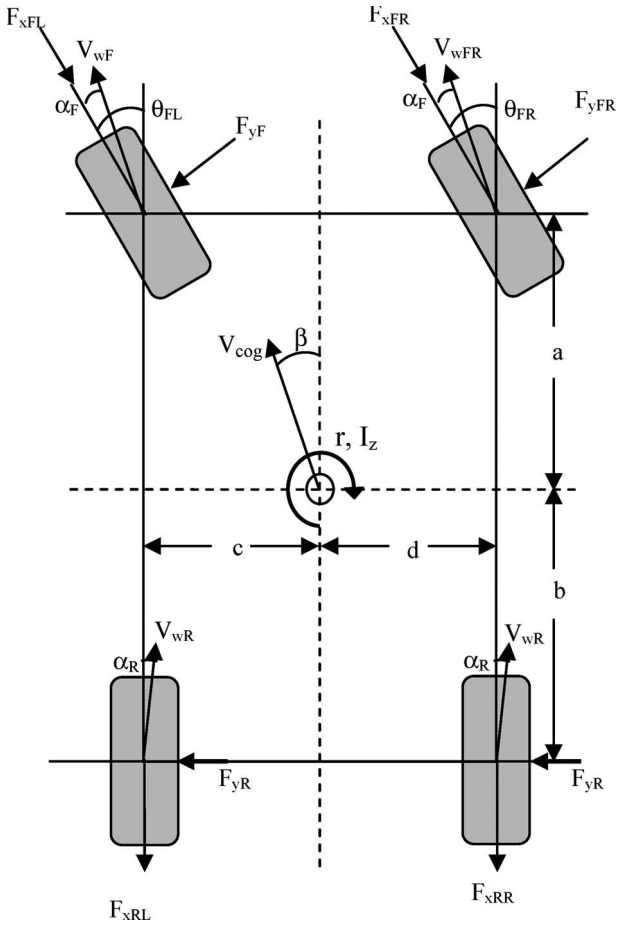

Fig. 4. Linear vehicle model.

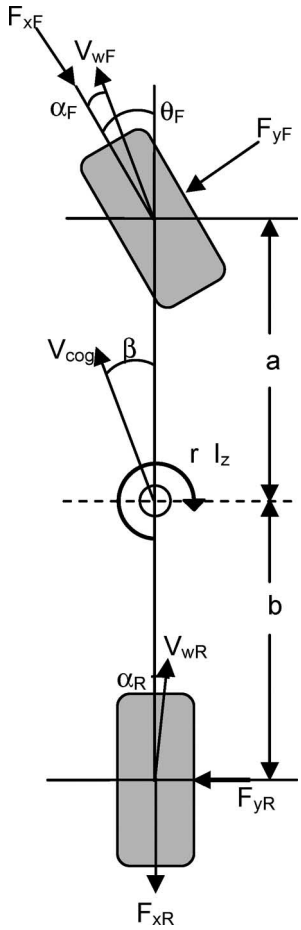

Fig. 5. Single-track vehicle model (bicycle model).

Here, k_a is assumed to be equal to 1. i_m is the input to the system, and τ_a and τ_f are treated as external disturbances. τ_f is given by

$$\tau_f = F_c \mathrm{sgn}(\dot{\theta}). \tag{5}$$

III. Linear Vehicle Model

Recalling (2), the disturbance torque τ_a is dependent on the front-tire sideslip angle. Assuming small sideslip angles (approximately less than 4°), the following equation can be used to approximate the front- and rear-tire sideslip angles [17]:

$$\begin{aligned} \alpha_F &= \beta + \frac{ar}{V} - \theta \\ \alpha_R &= \beta - \frac{br}{V} \end{aligned} \tag{6}$$

where

- θ RWA;
- β vehicle-body sideslip angle;
- r yaw rate;
- a distance from the front tire to the vehicle's center of gravity (CoG);
- b distance from the rear tire to the vehicle's CoG;
- V vehicle longitudinal velocity.

From (6), the sideslip angle is dependent on the vehicle states, namely the vehicle-body sideslip angle and the yaw rate. Fig. 4 illustrates the forces acting on the tires during a vehicle's turning maneuver. A two-track vehicle model can be derived based on this configuration. This two-track vehicle model can further be simplified to a single-track model or a bicycle model based on the symmetry of vehicle geometry. A linearized bicycle model (Fig. 5) will be used for the observer design to estimate the vehicle-body sideslip angle in this paper.

The following assumptions, which are generally good for normal driving maneuvers, are made These assumptions can significantly simplify the vehicle model.

- Assume that the friction forces in the x-direction are negligible when the vehicle is not braking.
- The left and right steering angles are approximately the same, i.e., $\theta_L = \theta_R = \theta$.
- For small angles, $\sin\theta = \theta$ and $\cos\theta = 1$.
- Assume vehicle symmetry, i.e., $c = d$.
- $F_{yFL} = F_{FR} = F_{yF}$ and $F_{yRL} = F_{yRR} = F_{yR}$.

With the aforementioned assumptions, the yaw dynamics of the vehicle is given by [17]

$$I_z \dot{r} = 2a(F_{yF}) - 2b(F_{yR}) \tag{7}$$

where

I_z	vehicle moment of inertia;
r	yaw rate;
$F_{xFL}, F_{yFL}, F_{xFR}, F_{yFR}, F_{xRL}, F_{yRL}, F_{xRR}, F_{yRR}$	tire contact forces in the longitudinal and lateral directions;
θ_L and θ_R	front and rear RWAs;
a, b, c, d	wheel contact location from the vehicle' CoG.

For small slip angles, the lateral forces F_{yF} and F_{yR} vary linearly with the tire slip angles and can be approximated by the following equation:

$$\begin{aligned} F_{yF} &= -C_{\alpha,f}\alpha_F \\ F_{yR} &= -C_{\alpha,r}\alpha_R \end{aligned} \tag{8}$$

where $C_{\alpha,f}$ and $C_{\alpha,r}$ are the front- and rear-tire cornering coefficients, which are the slope of the linear region on the lateral force versus slip angle plot.

Substituting (8) and (6) into (7), and rearranging terms, we get the following equation:

$$\dot{r} = \left(\frac{-aC_{\alpha,f} + bC_{\alpha,r}}{I_z}\right)\beta + \left(\frac{-a^2C_{\alpha,f} - b^2C_{\alpha,r}}{I_zV}\right)r + \left(\frac{aC_{\alpha,f}}{I_z}\right)\theta. \tag{9}$$

Next, the lateral dynamics of the vehicle can be obtained as follows: Making similar assumptions as aforementioned and assuming β to be a small angle, the following dynamic equation can be obtained [17]:

$$\dot{\beta} = \left(\frac{-C_{\alpha,f} - C_{\alpha,r}}{mV}\right)\beta + \left(-1 + \frac{-aC_{\alpha,f} + bC_{\alpha,r}}{mV^2}\right)r + \left(\frac{C_{\alpha,f}}{mV}\right)\theta. \tag{10}$$

Finally, combining (9) and (10) in a state-space form, the linear vehicle model is complete with vehicle-body sideslip angle and yaw rate as states. Equation (11) describes the complete vehicle. This model is also known as a single-track model or a bicycle model, as represented in Fig. 5. Thus

$$\begin{aligned} \dot{x} &= Ax + B\theta \\ x &= [\beta\ r]^T \\ A &= \begin{bmatrix} \frac{-C_{\alpha,f}-C_{\alpha,r}}{mV} & -1 + \frac{C_{\alpha,r}b - C_{\alpha,f}a}{mV^2} \\ \frac{C_{\alpha,r}b - C_{\alpha,f}a}{I_z} & \frac{-C_{\alpha,f}a^2 - C_{\alpha,r}b^2}{I_zV} \end{bmatrix} \\ B &= \begin{bmatrix} \frac{C_{\alpha,f}}{mV} \\ \frac{C_{\alpha,f}a}{I_z} \end{bmatrix}. \end{aligned} \tag{11}$$

A proportional–integral–differential controller was designed to control the road-wheel steer angle based on the aforementioned model.

IV. Body Sideslip Angle Observer and RWA Estimation

While the RWA sensors and yaw rate sensors are readily available on most vehicles, the vehicle-body sideslip angle cannot be measured directly. Instead, an observer is needed to estimate the vehicle-body sideslip angle. In Section III, the self-aligning torque τ_a is treated as a disturbance and then as a function of the vehicle states, namely the vehicle sideslip and the yaw rate. An observer can be designed by combining (4) and (11) with vehicle-body sideslip angle, yaw rate, steering angle, and steering rate as states of the vehicle, as illustrated in (12). The motor current is the input to the system, and the torque due to Coulomb friction is treated as a disturbance. Thus

$$\begin{aligned} \dot{x} &= Ax + Bi_m + E\tau_f \\ x &= [\beta \quad r \quad \theta \quad \dot{\theta}]^T \\ A &= \begin{bmatrix} \frac{-C_{\alpha,f}-C_{\alpha,r}}{mV} & -1+\frac{C_{\alpha,r}b-C_{\alpha,f}a}{mV^2} & \frac{C_{\alpha,f}}{mV} & 0 \\ \frac{C_{\alpha,r}b-C_{\alpha,f}a}{I_z} & \frac{-C_{\alpha,f}a^2-C_{\alpha,r}b^2}{I_zV} & \frac{C_{\alpha,f}a}{I_z} & 0 \\ 0 & 0 & 0 & 1 \\ \frac{(t_p+t_m)C_{\alpha,f}}{J_w} & \frac{a(t_p+t_m)C_{\alpha,f}}{J_wV} & \frac{-(t_p+t_m)C_{\alpha,f}}{J_w} & \frac{-b_w}{J_w} \end{bmatrix} \\ B &= \begin{bmatrix} 0 \\ 0 \\ 0 \\ \frac{k_m}{J_w} \end{bmatrix} \qquad E = \begin{bmatrix} 0 \\ 0 \\ 0 \\ \frac{-1}{J_w} \end{bmatrix} \\ C &= [0 \quad 0 \quad 1 \quad 0] \qquad C_T = [0 \quad 0 \quad 0 \quad 1] \\ C_B &= [1 \quad 0 \quad 0 \quad 0]. \end{aligned} \tag{12}$$

The observability matrix for the aforementioned system is given by

$$P_o = [C \quad CA \quad CA^2 \quad CA^3]. \tag{13}$$

It can be shown here that the aforementioned observability matrix has full rank. Hence, the aforementioned system is fully observable. The next step is to design a vehicle-body sideslip angle observer. This observer is based on a standard full-state observer methodology except that it includes the nonlinear disturbance term $F_c\mathrm{sgn}(\dot{\theta})$, as illustrated in Fig. 6. The observer gain vector L is designed to obtain critically damped observer error dynamics. By combining the vehicle-body sideslip angle observer with the SBW road-wheel system model, the road-wheel steering angle can be estimated, as illustrated in Fig. 7.

V. Sensor Dynamics

In the estimation of the road-wheel steer angle that was previously presented, the sensor dynamics has not been considered.

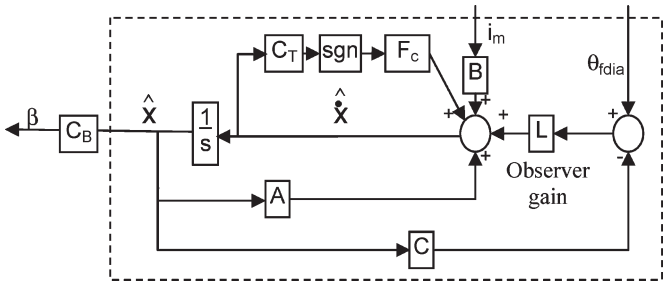

Fig. 6. Vehicle-body sideslip angle observer.

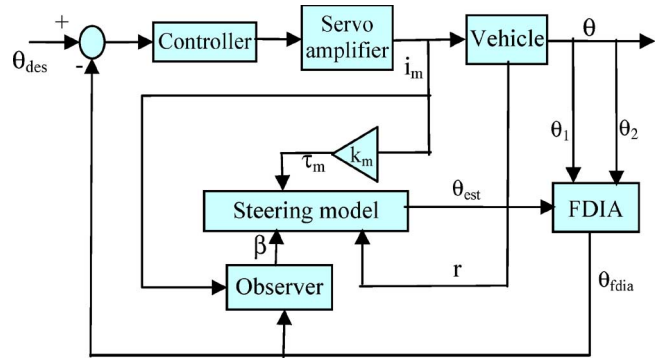

Fig. 7. RWA estimation and FDIA.

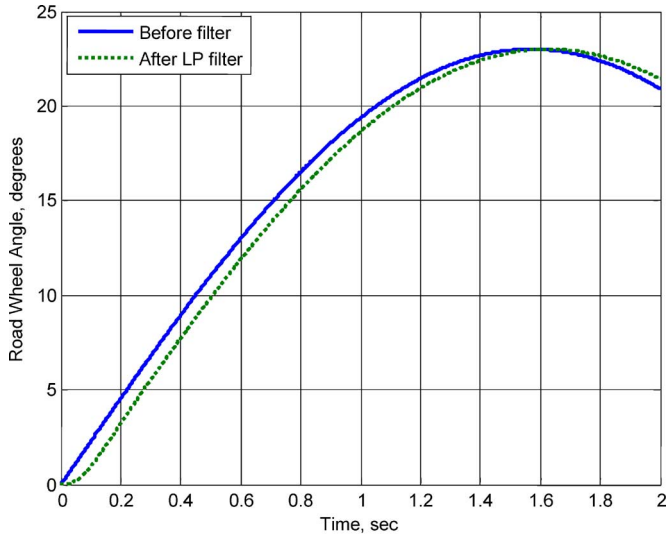

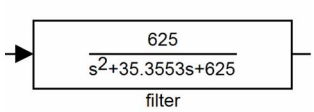

Fig. 8. Butterworth filter design.

In this section, we include the influence of sensor dynamics on the overall estimation accuracy. An analog Butterworth filter was used to model the motor-current sensor dynamics. Using a cutoff frequency $\omega_n = 25$ Hz, a second-order low-pass filter is designed. The numerator and denominator of the filter transfer function are determined using the appropriate MATLAB function. Fig. 8 shows the delayed response due to the motor-current sensor dynamics. The observer, the controller, and the filter are integrated in system model, as shown in Fig. 9.

VI. Analytical Redundancy

The vehicle states, including the vehicle-body sideslip angle, can be estimated via an observer, as presented in the previous sections. Thus, the road-wheel steer angle can be estimated from the measured yaw rate, the estimated vehicle-body sideslip angle, the measured steering motor current, and θ_{fdia}. This effectively adds another RWA position value for the ECU to compare against the physical position sensors. The more analytical position values compared, the more robust the system is, but at a greater computational cost. For this reason, we only consider three RWA sensor signals: one from analytical redundancy and two from physical sensors, possibly a combination of an absolute position sensor and a relative position sensor. Elimination of a physical RWA sensor without compromising reliability will help bring SBW system a step closer to reality by reducing the overall system cost. This paper is focused on RWA sensor redundancy via analytical methods. However, an actual SBW system would also require redundant actuators, power supplies, ECUs, and communication networks (Fig. 1).

VII. FDIA

In order for the SBW system to be robust, the sensor measurements must be accurate and reliable. Therefore, any faulty signal must be eliminated to prevent undesirable steering effects. The FDIA algorithm developed in this paper is able to handle a single-point fault without interrupting the functionality of the SBW system. This algorithm can be easily modified to handle multiple faults if more than three sensor signals are compared. The FDIA algorithm implemented in SIMULINK is based on a majority voting scheme in which a minimum of three signals are required for this scheme to work. The sensor signals are compared against each other in real time to determine the faulty signal where majority is assumed to be correct. This is based on the assumption that the event of a sensor failure is rare and the event of multiple simultaneous sensor failures is extremely rare. This algorithm can determine which sensor has failed by comparing its value against other sensors' values. This algorithm can manage hard failures as well as soft failures. Hard failure is characterized by an abrupt or sudden sensor failure, and soft failure is characterized by biases or drifts in the signal over time. If one sensor fails, then its output would be different from the other two. Likewise, the other two working sensors would have very similar outputs, which are different from the failed sensor. When a sensor fails, its signal is no longer used in the RWA calculation. In such a situation, the driver would be alerted of the sensor failure and would still be able to maintain safe control of the vehicle.

In this investigation, only three signal values have been used, but more signals can be easily implemented if a higher level of reliability is desired. The FDIA algorithm has been implemented using finite-state machine logic (StateFlow) in SIMULINK, as shown in Fig. 10. The three sinusoidal signals

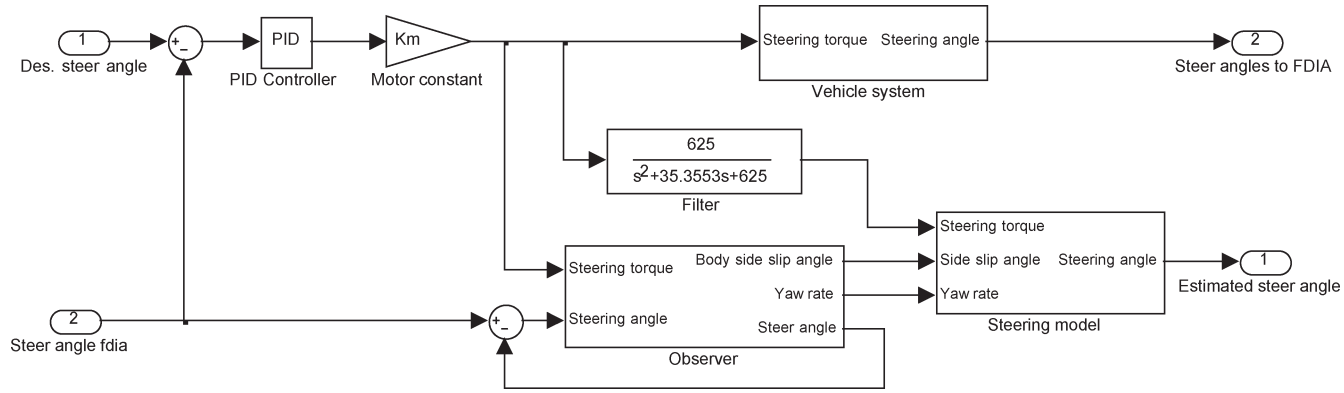

Fig. 9. Combined observer and steering system model.

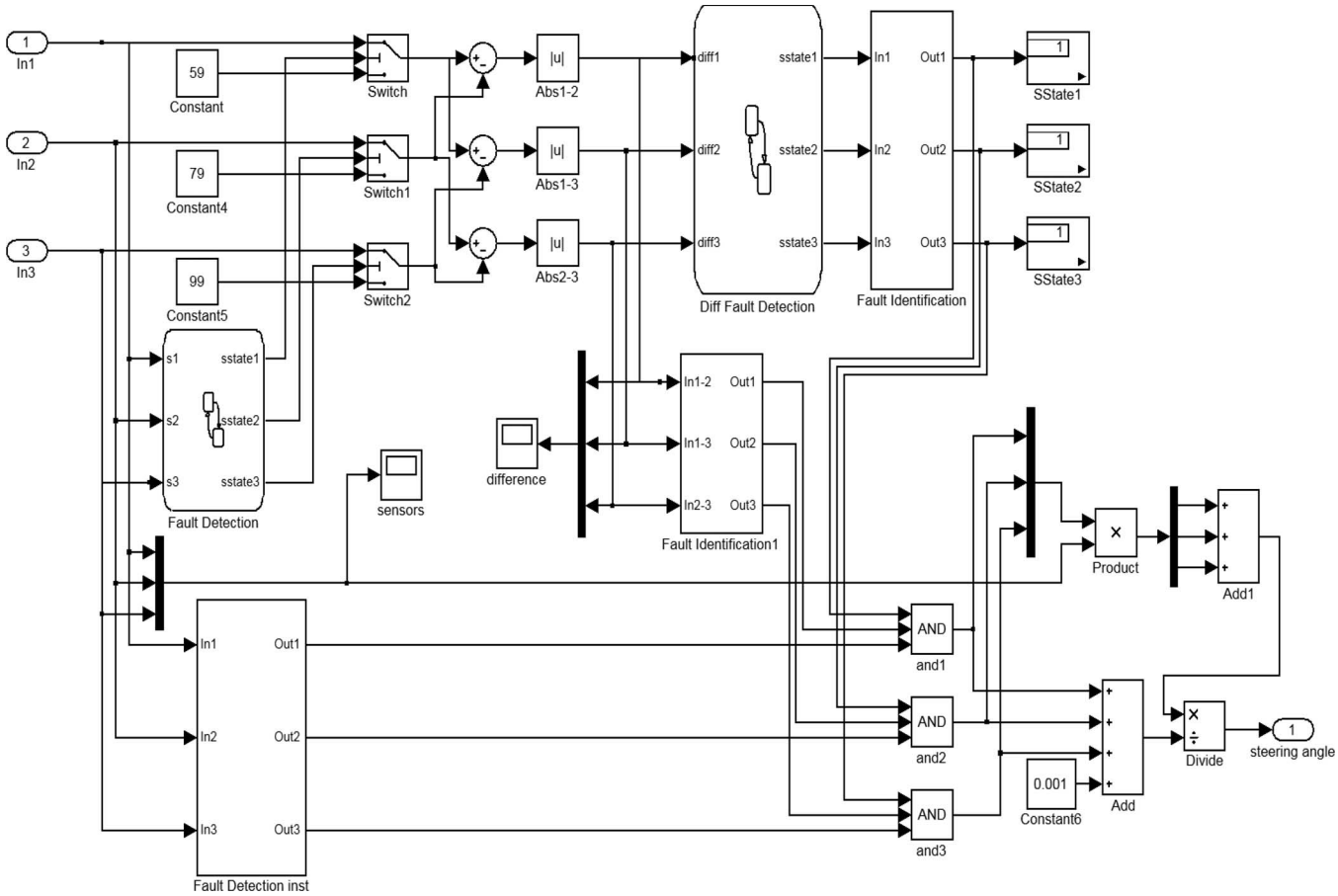

Fig. 10. FDIA algorithm.

representing steering angles first go through the fault detection block, where it is checked to see if it is within the allowable range of operation. If it falls outside of this range, a 0 flag is set, indicating a failed sensor; otherwise, a 1 is set. For example, if a sensor indicates the RWA is 90°, which is impossible for conventional vehicles, then the sensor is giving false readings, and a 0 flag is set. Fig. 11 shows the state flow diagram for the fault detection block. Initially, the state of the signal is set to good or 1. If it encounters an out of range value, the state will be set to failed or 0. However, there may be disturbances from the system or the environment that may cause short-term transient errors. To prevent this short transient error from causing the sensor to be considered faulty, a time delay is used. Therefore, the error has to persist for a specified length of time, as determined by a counter loop, before it can be declared a real sensor failure. If the sensor recovers from the transient error within that time, then the sensor maintains the 1 flag; otherwise, a 0 flag is set. The counter is a tunable parameter that can be varied depending on the operating conditions and needs.

If the signal failed from the first fault detection block, it will be assigned an arbitrary large constant. This large constant

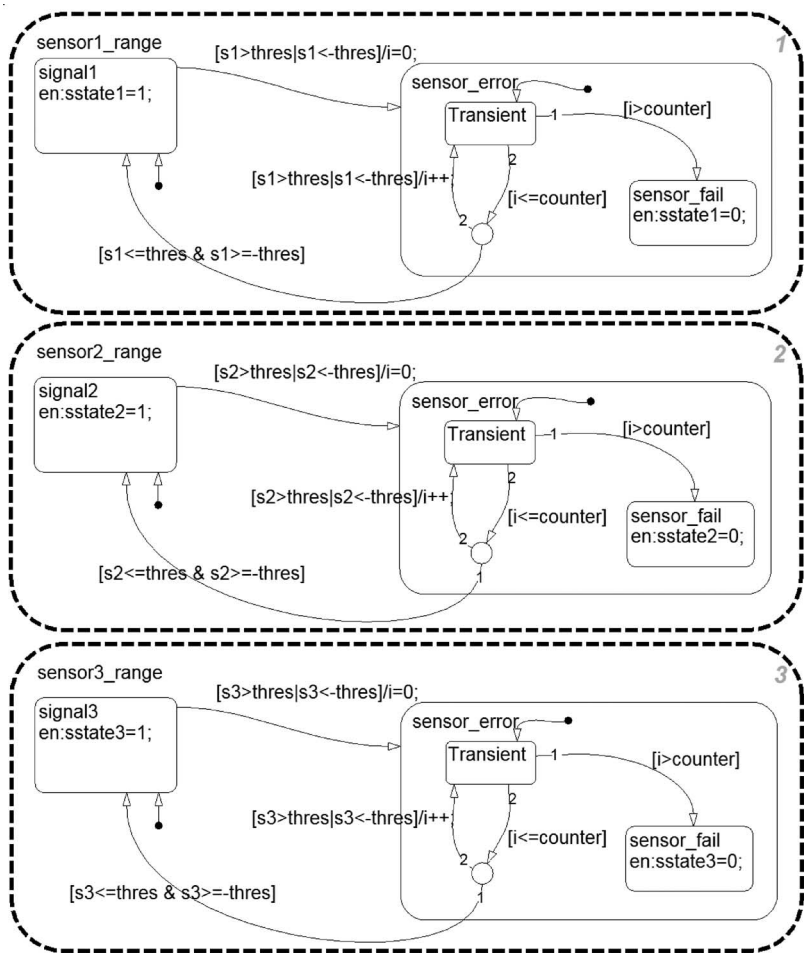

Fig. 11. Fault detection state flow model.

will guarantee that the signal will also fail the next phase of fault detection. The signals or constants are then subtracted from each other to obtain the difference values. The "Diff Fault Detection" block will identify the fault based on the difference values: (signal1–signal2), (signal1–signal3), and (signal2–signal3). These values are compared against a difference threshold to determine whether the difference is acceptable. The difference threshold is a tunable parameter to allow a reasonable level of discrepancy due to system and environment noise. The state flow for the Diff Fault Detection block works very similarly to the first fault detection block. If the difference value is beyond the difference threshold for a specified length of time, a 0 flag is set to indicate the difference value as a failed state. The fault has to persist for a specified number of loops before it can be declared as a real fault; otherwise, it will return to a 1 state. The number of loops is also a tunable parameter based on operating conditions and user preference.

After the second fault detection block, the difference values are flagged as either 1 for being within the threshold value or as 0 for exceeding the threshold value. From this output, a truth table can be used to identify the faulty sensor. If all the values are 1, then they are all within the threshold of each other, and all the signals are correct. If the first and second values are 0 and the third value is 1, then signal1 has failed. The same logic applies to signal2 and signal3 failures. This fault logic is captured in a truth table (Table I). The table will be all 0 if two or more sensors fail. The conditions where the difference between the highest and the lowest signals fall outside of the difference threshold range but are both close to the middle signal can be described by the last three rows of the table. All three signals would be considered good, and the average would produce a result close to the middle signal. This truth table can be easily implemented using OR logic gates, as shown in Fig. 12. The truth table can be easily expanded to include more than three signals if necessary. Finally, the states of the signals, i.e., 0 or 1, are multiplied with the value of the signal. These values are summed and averaged by the number of signals with 1 state to produce the RWA.

To eliminate the transient errors from causing false sensor failures, state flow blocks with time delays have been used. However, this still allows the transient errors to be averaged into the final calculation and to produce discontinuities. These discontinuous transient errors are very undesirable and could be detrimental to the actuators. To prevent this, parallel FDI blocks are included (Figs. 13 and 14). These blocks work similar to the previous error detection blocks. The only difference is that it does not wait for the error to persist for a specified time

TABLE I
SENSOR FAULT TRUTH TABLE

(Sensor1 – Sensor2)	(Sensor1 – Sensor3)	(Sensor2 – Sensor3)	Fault Decision
1	1	1	Fault free case
0	0	1	Sensor 1 fault
0	1	0	Sensor 2 fault
1	0	0	Sensor 2 fault
0	0	0	2 or more sensor fault
0	1	1	Fault free case
1	0	1	Fault free case
1	1	0	Fault free case

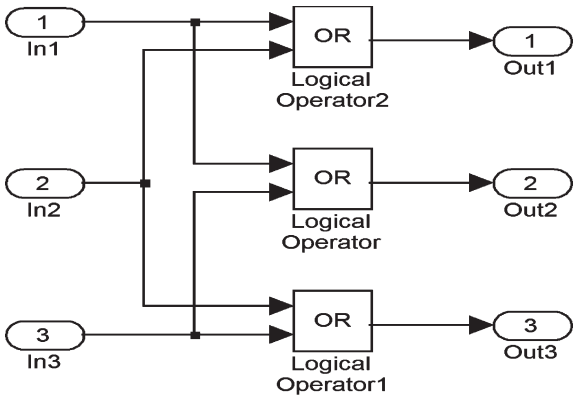

Fig. 12. Fault detection logic.

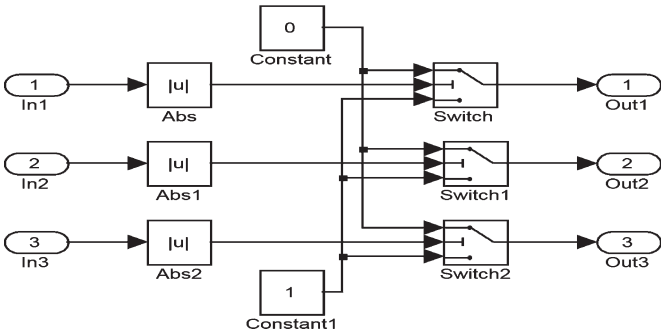

Fig. 13. Transient fault detection.

period before declaring faulty signal. Instead, when an error is encountered, the error flag is set right away to prevent the error from being included in the final calculation.

VIII. SIMULATION RESULTS

As indicated in Section I, a number of simulation runs were performed to evaluate the developed algorithms presented in this paper. The SBW controller, the body sideslip angle observer, the RWA estimator, and the FDIA algorithms are combined with a simplified vehicle model with an SBW actuation system. The combined model was given a sinusoidal steering input. Fault was then injected to one of the three RWA sensors (one analytical). Fault flags and the output of the RWA from the FDIA block are then recorded. Fig. 15 shows three test signals varying in phase and magnitude, including one with transient pulses (transient fault). The differences in magnitude are all within the allowable threshold, and the short-term pulses are also within the allowable time. Therefore, the states of all the signals are considered good. The pulses are eliminated, and the signals are averaged to produce a smooth curve (Fig. 16), indicating the effectiveness of the proposed algorithms.

The following values for the vehicle parameters have been considered for the preliminary simulation runs:

$$C_{\alpha,f} = 23,000 \text{ N/rad} \qquad C_{\alpha,r} = 46,000 \text{ N/rad}$$
$$m = 1961 \text{ kg} \qquad V = 13.4 \text{ m/s}$$
$$a = 1.05 \text{ m} \qquad b = 1.71 \text{ m}$$
$$I_z = 3136 \text{ kg} \cdot \text{m}^2 \qquad k_m = 0.2$$
$$t_p = 0.0381 \text{ m} \qquad t_m = 0.04572 \text{ m}$$
$$J_w = 3.5 \text{ kg} \cdot \text{m}^2.$$

In Fig. 17, a persistent fault was injected into one of the RWA signals by making the sensor send out a constant value. It was considered a faulty signal by the FDIA block and was eliminated from the FDIA block output. The RWA (Fig. 18) is the average of the two working signals.

As evident from the simulation results that were previously presented, the analytical redundancy-based FDIA algorithm developed in this paper have been effective in maintaining the reliability of SBW system as it would have been with full hardware redundancy. It should be noted, however, that if two signals become faulty (simultaneous double failure), this algorithm would not be able to distinguish the good sensor from

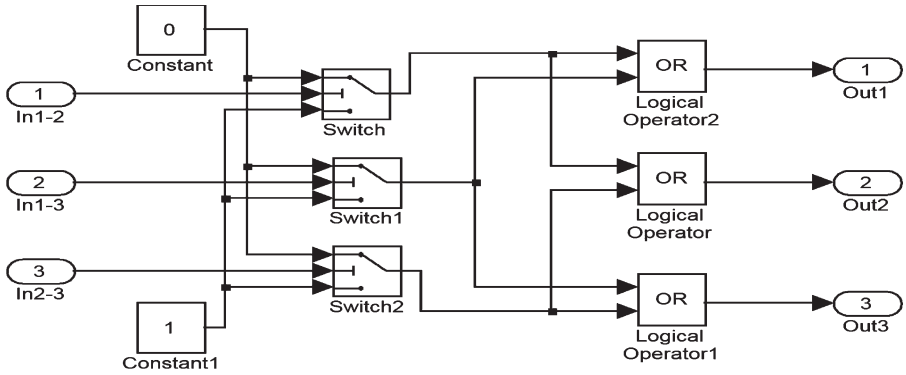

Fig. 14. Fault detection and isolation.

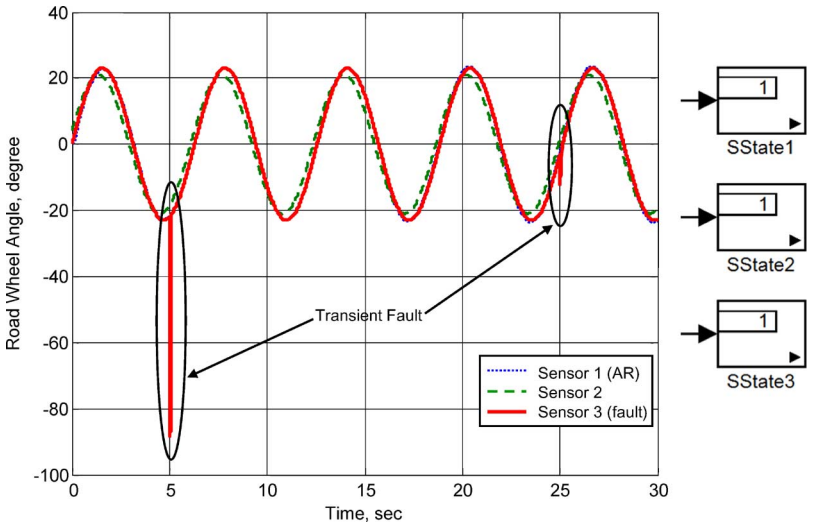

Fig. 15. Transient fault introduced in one of the two physical sensors with the fault state displayed on the right.

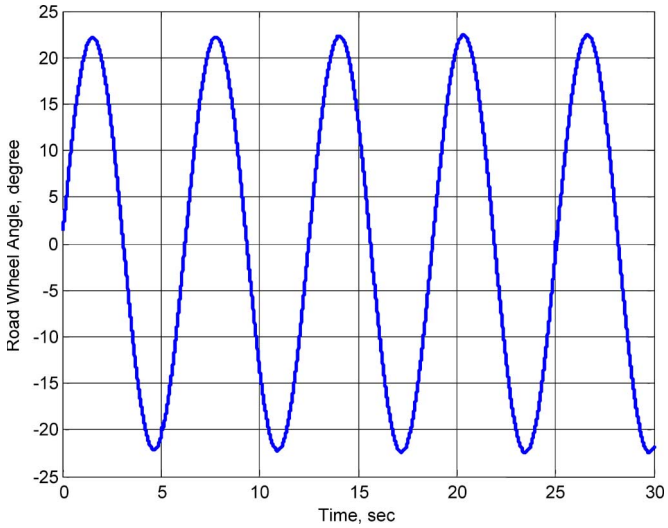

Fig. 16. FDIA output of sensor data after removing the transient fault in one physical sensor.

the bad sensors and will consider all three failed and will not produce any steering angle since the proposed methodologies are based on the assumption of only single-point failure.

The aforementioned simulation results thus show that the analytical redundancy methods that are proposed here successfully detected both types of faults and provided the SBW controller with the correct values of the RWA.

While the simulation results presented in this paper illustrate the effectiveness of the proposed analytical redundancy-based algorithms, experimental validation of these algorithms on a real SBW vehicle would further establish the accuracy and robustness of the proposed algorithms. A hardware-in-loop (HIL) bench consisting of an SBW system with redundant hardware components that communicates with a real-time vehicle model would also be an appropriate platform to validate the analytical redundancy-based algorithms presented here. The authors have taken this approach in validating the findings in this paper. The HIL bench is currently under construction.

IX. Conclusion

We presented a novel method for analytical redundancy-based FDIA for an SBW system in this paper. A full-state observer was designed using the combined steering system model and vehicle model to estimate the vehicle-body sideslip angle. With the states of the vehicle thus known, the RWA position could be estimated. The accuracy of the estimate depends on the accuracy of the model and the observer. Through the proposed model-based fault detection methodology, an extra level of redundancy without extra hardware was possible.

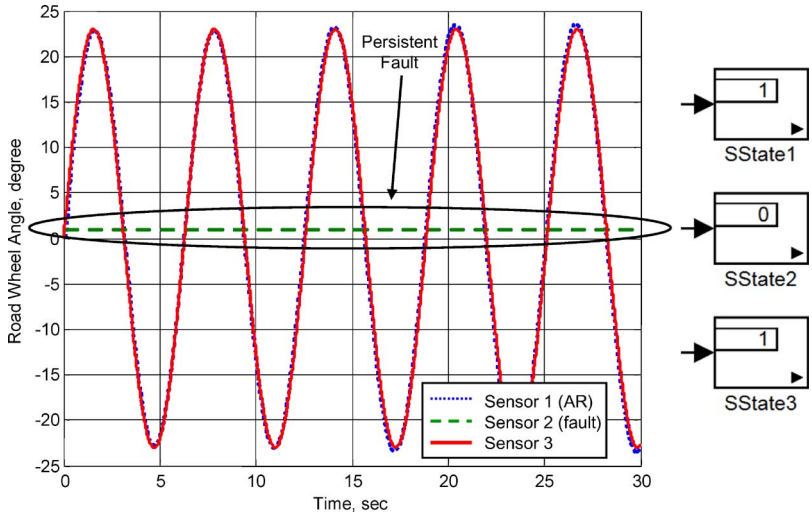

Fig. 17. Persistent sensor fault introduced in one of the two physical sensors with the fault state displayed on the right.

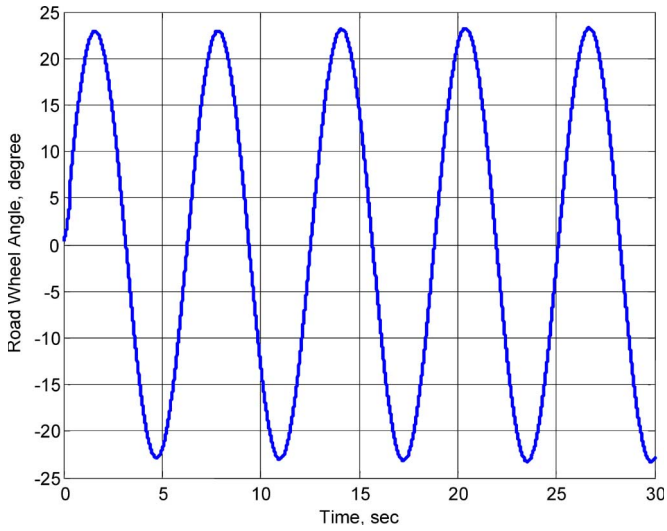

Fig. 18. FDIA output of sensor data after removing the persistent fault in one physical sensor.

We also presented a fault-tolerant algorithm for single-point faults. Through a majority voting scheme and a minimum of three sensors, this algorithm is able to identify the faulty sensor(s) and prevent it (them) from causing errors in the steering position. If a sensor error occurs, the algorithm will automatically route the control to only accept signals from the two functional sensors. The driver will still be able to control the vehicle normally with only two sensors.

It is thus demonstrated that it is possible to at least maintain the level of reliability of the hardware redundancy via the proposed analytical redundancy methodologies.

REFERENCES

[1] S. Frauzen, "Safety and usability benefits of steer-by-wire systems," in *Proc. 26th Int. Symp. Automot. Technol. Autom. Road Veh. Safety*, Aachen, Germany, Sep. 13–17, 1993, pp. 63–71.

[2] R. Isermann, R. Schwarz, and S. Stolzl, "Fault-tolerant drive-by-wire systems," *IEEE Control Syst. Mag.*, vol. 22, no. 5, pp. 64–81, Oct. 2002.

[3] R. Isermann, "Diagnosis methods for electronic controlled vehicles," *Veh. Syst. Dyn.*, vol. 36, no. 2/3, pp. 77–117, Sep. 2001.

[4] B. Zheng, C. Altemare, and S. Anwar, "Fault tolerant steer-by-wire road wheel control system," in *Proc. Amer. Control Conf.*, Portland, OR, Jun. 8–10, 2005, pp. 1619–1624.

[5] S. E. Muldoon, M. Kowalczyk, and J. Shen, "Vehicle fault diagnostics using a sensor fusion approach," in *Proc. IEEE Sens.*, 2002, vol. 1, pp. 1591–1596. n 2.

[6] Y. Gao and H. F. Durrant-Whyte, "Multi-sensor fault detection and diagnosis using combined qualitative and quantitative techniques," in *Proc. IEEE Int. Conf. Multisensor Fusion Integr. Intell. Syst.*, 1994, pp. 43–50.

[7] S. You and L. Jalics, *Hierarchical Component-Based Fault Diagnostics for By-Wire Systems*, 2004. SAE Tech. Paper Series 2004-01-0285.

[8] M. Stanek, M. Morari, and K. Frohlich, "Model-aided diagnosis: An inexpensive combination of model-based and case-based condition assessment," *IEEE Trans. Syst., Man, Cybern. C, Appl. Rev.*, vol. 31, no. 2, pp. 137–145, May 2001.

[9] R. Rengaswamy, D. Mylaraswamy, K. E. Arzen, and V. Venkatasubramanian, "A comparison of model-based and neural network-based diagnosis methods," *Eng. Appl. Artif. Intell.*, vol. 14, no. 6, pp. 805–818, Dec. 2001.

[10] M. Hashimoto, H. Kawashima, and F. Oba, "A multi-model based fault detection and diagnosis of internal sensor for mobile robot," in *Proc. IEEE Int. Conf. Intell. Robots Syst.*, 2003, vol. 4, pp. 3787–3792.

[11] A. Wernz and K. Kroschel, "Instrument fault detection and identification based on analytical redundancy," *IFAC Fault Detection, Supervision and Safety for Technical Processes*, 1991, Baden-Baden, Germany.

[12] N. Venkateswaran, M. S. Siva, and P. S. Goel, "Analytical redundancy based fault detection of gyroscopes in spacecraft applications," *Acta Astronaut.*, vol. 50, no. 9, pp. 535–545, 2002.

[13] H. Suzuki, T. Kawahara, S. Matsumoto, Y. Ikeda, H. Nakagawa, and R. Matsuda, "Fault diagnosis of space vehicle guidance and control systems using analytical redundancy," *Space Technol.*, vol. 19, no. 3/4, pp. 173–178, 1999.

[14] Y. Dong and Z. Hongyue, "Optimal design of robust analytical redundancy for a redundant strapdown inertial navigation system," *Control Eng. Pract.*, vol. 4, no. 12, pp. 1747–1752, 1996.

[15] R. W. Kelly, "Application of analytical redundancy to the detection of sensor faults on a turbofan engine," in *Proc. ASME Int. Gas Turbine and Aeroengine Congr. Expo.*, Birmingham, U.K., Jun. 10–13, 1996, pp. 1–8.

[16] J. O. Hahn, S. H. You, Y. M. Cho, S. Kang, and K. I. Lee, "Fault diagnostics in the differential brake control system using the analytical redundancy technique," in *Proc. 42nd IEEE Conf. Decision Control*, Maui, HI, Dec. 2003, pp. 2276–2281.

[17] S. Anwar, "Generalized predictive control of yaw dynamics of a hybrid brake-by-wire equipped vehicle," *Int. J. Mechatron.*, vol. 15, pp. 1089–1108, Nov. 2005.

Sohel Anwar received the Ph.D. degree in mechanical engineering from the University of Arizona, Tucson, in 1995.

In 1995, he joined Caterpillar, Inc., Peoria, IL, as a Research Engineer, where he was responsible for developing advanced control systems for Earth-moving equipment. From 1999 to 2004, he was a Senior R&D Engineer with Visteon Corporation, Dearborn, MI, where he led projects in the area of control system development for drive-by-wire systems. Since 2004, he has been with the Department of Mechanical Engineering, Purdue School of Engineering and Technology, Indiana University-Purdue University Indianapolis, Indianapolis, IN, as an Assistant Professor. He is the holder of 12 U.S. patents.

Dr. Anwar is a member of the American Society of Mechanical Engineers and a Faculty Advisor for the Society of Automotive Engineers International. He is a Registered Professional Engineer in the State of Michigan.

Lei Chen received the M.S. degree in electrical engineering from Indiana University-Purdue University Indianapolis, Indianapolis, IN, in 2006.

He is currently with a private firm in California.